

Modeling and Analysis of Single-Plate Shear Connections Under Column Loss

Joseph A. Main, Ph.D., A.M.ASCE¹ and Fahim Sadek, Ph.D., M.ASCE²

Abstract: This paper presents a computational assessment of the behavior of single-plate shear (“shear tab”) connections in gravity frames under column loss scenarios. Two-span beam assemblies without floor slabs are considered under push-down loading of the unsupported center column. Both detailed and reduced modeling approaches are used in the computational assessment, and comparisons with experimental data are presented to establish confidence in the models. The models are used to investigate the influence of factors such as end support conditions, span length, connection strength, and post-ultimate connection behavior on the collapse resistance of gravity framing systems. Rotational capacities of single-plate shear connections under column loss scenarios are found to be in some cases less than half of the values based on seismic test data, due to the axial extension imposed on the connections in addition to rotation.

CE Database subject headings: Buildings; Connections; Finite element method; Nonlinear analysis; Progressive collapse; Steel structures.

Introduction

Computational studies (Sadek et al. 2008, Alashker et al. 2010) have indicated the susceptibility to collapse of gravity frames (i.e., frames designed to carry only vertical loads) with single-plate shear connections (also known as “shear tab” or “fin plate” connections) under column loss. The composite floor slab was found to significantly enhance the capacity of the system relative to that of the bare steel framing. However, the capacity of the composite system was still found to be inadequate to sustain

¹ Research Structural Engineer, Engineering Laboratory, National Institute of Standards and Technology, Gaithersburg, MD 20899-8611 (corresponding author). E-mail: joseph.main@nist.gov

² Leader, Structures Group, Engineering Laboratory, National Institute of Standards and Technology, Gaithersburg, MD 20899-8611. E-mail: fahim.sadek@nist.gov

gravity loads under sudden column loss. To investigate the collapse resistance of gravity frame systems, recent and ongoing experimental studies (Thompson 2009, Oosterhof and Driver 2012, Weigand et al. 2012) have assessed the behavior of single-plate shear connections under combinations of shear force, bending moment, and axial tension representative of column loss scenarios.

The collapse-resistance of single-plate shear connections depends on a number of factors, including span length, connection strength (e.g., number of bolts), and post-ultimate behavior. Sadek et al. (2008) and Alashker et al. (2010) considered a bay size of 6.10 m \times 9.14 m, where the 6.10 m span is somewhat short compared to typical construction. Longer beam spans might be expected to impose greater demands on the connections under column loss scenarios, potentially leading to increased susceptibility to collapse. Sadek et al. (2008) and Alashker et al. (2010) considered connections governed by tear-out failure, characterized by gradual softening in the post-ultimate response. However, tests by Thompson (2009) and Weigand et al. (2012) exhibited sudden fracture, associated with bolt shear rupture or brittle plate rupture, resulting in a loss of both axial and shear capacity at a smaller rotation than would be sustained due to gradual softening. Models that accurately capture the influences of these factors are important for assessing the capacity of gravity framing systems under column loss.

Motivated by these considerations, this paper presents modeling and analysis of two-span beam assemblies with single-plate shear connections under “push-down” loading, as illustrated in Fig. 1. Two finite element modeling approaches for the connections are presented: (1) detailed modeling, which uses solid elements, plasticity models, and contact algorithms, and (2) reduced modeling (also known as a “component-based” or “macromodel-based” approach), which uses assemblies of beam and nonlinear spring elements. A number of previous studies have used computational modeling to study the behavior of single-plate connections. Sarraj (2007) developed both detailed and reduced models to study the behavior of single-plate connections under fire-induced heating. Sadek et al. (2008) presented empirical equations for reduced modeling of single-plate connections under column loss and compared detailed and reduced model results. Daneshvar and Driver (2011) compared detailed model results with experimental

results from Thompson (2009). Yim and Krauthammer (2012) presented detailed and reduced models to represent the moment-rotation behavior of single-plate connections.

The reduced modeling approach presented in this paper extends the empirical model of Sadek et al. (2008) by incorporating vertical shear deformation and failure, connection slippage, inelastic unloading behavior, and sudden fracture, as applicable. Both detailed and reduced models are analyzed using explicit time integration in LS-DYNA (Hallquist 2007), with displacement-controlled loading applied slowly to achieve a quasi-static response. Comparisons of both detailed and reduced models with experimental data from Thompson (2009) are presented to develop confidence in the modeling approaches. Detailed and reduced models are then used to analyze two-span beam assemblies from the gravity framing systems of prototype buildings described in Main and Sadek (2012), and the influences of support conditions, span length, connection strength, and post-ultimate behavior on the ultimate load and rotational capacities of the assemblies are investigated.

Detailed Modeling

The detailed modeling approach for single-plate shear connections, illustrated in Fig. 2, uses solid elements to represent the beam, plate, and bolts, with typical element sizes of 1.5 mm for the bolts and 3 mm for the beam and plate. Contact is defined between the bolts, plate, and beam web to model the transfer of forces through the bolted connection, including friction and bolt bearing. A piecewise-linear plasticity model (material 24 in LS-DYNA) is used to represent the material behavior of the various steel components. In this material model, an effective stress versus effective plastic strain curve is specified, along with a plastic strain to failure, at which elements are removed from the model to simulate fracture. The material model parameters for each component were developed based on engineering stress-strain curves obtained from tensile tests reported in the literature for each type of steel. The engineering stress-strain curves were converted to true stress vs. plastic strain curves, which were extrapolated linearly beyond the point of necking onset. The post-necking modulus and the failure strain were adjusted so that engineering stress-strain curves obtained from finite element models of tensile coupons would correspond

closely to the coupon test results. Due to mesh-size sensitivity in the modeling of softening behavior, this calibration was performed using finite element models of tensile coupons with the same mesh size as those used in the models of each connection.

For the ASTM A325 high-strength bolts, the material model parameters were based on a typical engineering stress-strain curve from coupon testing reported in Kulak et al. (1986) and shown in Fig. 3(b) (labeled “coupon test”). The corresponding true stress-strain curve evaluated from the coupon test data is shown in Fig. 3(a). Note that the true stress-strain curve exhibits a drop in stress at a plastic strain of about 8 %, which corresponds to the onset of necking; extrapolation was needed beyond this point because the coupon data are not representative of the true stress in the neck region of the coupon. The extrapolated true stress-strain curve, labeled “model” in Fig. 3(a), was implemented in a solid-element model of a tensile coupon with a gage length of 50 mm, shown in the inset of Fig. 3(b). The engineering stress-strain curve computed from the coupon model is shown in Fig. 3(b) along with the coupon test results. The good comparison of the computed and experimental stress-strain curves in Fig. 3(b) shows that the piecewise linear plasticity model with element erosion accurately captures softening behavior after the onset of necking and fracture at the appropriate elongation. A similar procedure to that illustrated in Fig. 3 was used to calibrate the plasticity model for the A36 and A992 steel materials used for the plate and wide-flange components, respectively, with values of yield strength, tensile strength, and percent elongation corresponding to the minimum values in the ASTM specifications (Fig. 4).

To develop confidence in the detailed modeling approach, model predictions were compared with available experimental data from connections with a single bolt, including double-shear tests (Wallaert and Fisher 1965), a test of bolt bearing on a single plate (Rex and Easterling 2003), and a single-shear test (Richard et al. 1980). These comparisons, presented in Main and Sadek (2012), showed that detailed models are able to capture both bolt shear deformations and bearing-induced plate deformations, including the combination of these mechanisms that contributes to the overall deformation in single-plate shear connections.

Reduced Modeling

The reduced modeling approach for single-plate shear connections, illustrated in Fig. 5, uses biaxial springs, one for each bolt row in the connection, with distinct load-deformation curves to represent yielding and failure (1) along the beam axis and (2) in vertical shear. The biaxial springs are implemented using a zero-length discrete beam element formulation (beam type 6 with material 119 in LS-DYNA). To maintain the proper connection geometry, rigid links connect the ends of the spring elements to nodes along the beam and column centerlines.

Alternate axial load-deformation relationships are shown in Fig. 6, in which forces and deformations along the beam axis are plotted on the vertical and horizontal axes, respectively. Positive values of deformation (corresponding to tensile forces) denote displacements away from the column. Note that both tensile and compressive forces in a connection spring (or bolt row) are developed through shear forces in the bolt itself. Fig. 6(a) shows a load-deformation relationship of the form proposed by Sadek et al. (2008) for axial behavior controlled by bolt tear out, which exhibits a gradual drop in resistance after the ultimate load in tension (t_u) is reached and no drop in resistance after the ultimate load in compression (c_u) is reached. The load-deformation relationship in Fig. 6(b) exhibits a steeper drop in resistance after the ultimate load is reached in both tension and compression and is applicable for axial behavior controlled by bolt shear failure. As is discussed subsequently, it is recommended that a load-deformation relationship of the form in Fig. 6(b) be conservatively assumed in the analysis of single-plate shear connections.

In both cases, the initial stiffness k of the connection spring is estimated based on a linear regression of rotational stiffness data from seismic testing. The initial rotational stiffness of a single-plate shear connection, here denoted κ , is given in Eq. (5-19) of FEMA 355D (FEMA 2000):

$$\kappa = 124\,550(d_{bg} - 142 \text{ mm}) \quad (\text{kN} \cdot \text{mm}/\text{rad}) \quad (1)$$

where $d_{bg} = s(N - 1)$ is the depth of the bolt group, $s = 76.2$ mm is the vertical spacing between bolts, and N is the number of bolts. The initial translational stiffness of a spring element representing a single bolt row, denoted k , can then be estimated as:

$$k = \frac{\kappa}{\sum_i y_i^2} \quad (2)$$

where y_i is the vertical distance of the i th bolt row from the center of the bolt group.

The yield and ultimate capacities of each spring in tension (t_y and t_u , respectively) and in compression (c_y and c_u , respectively) are calculated based on the governing failure mode of the connection under axial loading, using equations in the AISC Specification (AISC 2010) with a resistance factor of $\phi = 1$. Minimum specified values of yield strength F_y and ultimate strength F_u for each type of steel are used in these equations. Axial connection capacities are divided by the number of bolts to obtain the capacity of a single bolt row. While other failure modes may potentially govern (e.g., fillet weld failure or block shear failure), the governing failure modes for the single-plate shear connections in this study are bearing failure at bolt holes (AISC 2010, Section J3.10) and bolt shear failure (AISC 2010, Section J3.6). Equations for the yield and ultimate capacities in these limit states are listed in Table 1, in which t is the thickness of the connected material (beam web or plate), L_c is the clear distance between the edge of the bolt hole and the edge of the connected material, and d and A_b are the diameter and cross-sectional area of the bolt, respectively (see AISC 2010). The ultimate strength of the bolt in shear is denoted F_v . Values of F_v listed in the footnote of Table 1 were obtained by dividing the values reported in Table 5.1 of the Research Council on Structural Connections Specification (RCSC 2004) by a factor of 0.80 to eliminate the reduction in strength that accounts for non-uniform shear force distribution, since for axial loading the connections under consideration have only one bolt in the line of force. The factor of 0.75 in the expression for the bolt shear yield capacity is the approximate ratio of the yield strength to the ultimate strength of the bolts.

The spring displacement corresponding to the ultimate load, denoted δ_u , is estimated using Eq. (5-17a) in FEMA 355D (FEMA 2000), which gives the plastic rotational capacity of simple shear connections designed using the AISC Specifications, and with adequate clearance between beam flanges from column to prevent binding. Adding an estimated elastic rotation of 0.02 rad to Eq. (5-17a) from FEMA 355D gives the following estimated total rotational capacity (in rad):

$$\theta_{max} = 0.17 - 0.00014d_{bg} \quad (d_{bg} \text{ in mm}) \quad (3)$$

Since the tests in FEMA 355D (FEMA 2000) subjected the connections to rotation with no axial extension, the deformation at ultimate load for a connection spring element can be estimated as

$\delta_u = y_{max}\theta_{max}$, where $y_{max} = d_{bg}/2$ represents the distance from the center of the bolt group to the most distant bolt. Substituting Eq. (3) for θ_{max} yields the following expression for δ_u :

$$\delta_u = 0.085d_{bg} - 0.00007d_{bg}^2 \quad (d_{bg} \text{ in mm}) \quad (4)$$

Note that while θ_{max} decreases with d_{bg} , δ_u actually increases with d_{bg} , from $\delta_u = 11.3$ mm for $d_{bg} = 152.4$ mm (a 3-bolt connection) to $\delta_u = 19.3$ mm for $d_{bg} = 304.8$ mm (a 5-bolt connection). The increase of δ_u with d_{bg} , follows directly from Eq. (3), which represents a fit to experimental data. The experimental data thus indicate that deeper connections can accommodate larger deformations prior to failure.

For axial behavior characterized by gradual softening due to tear-out failure [Fig. 6(a)], the failure displacement of the spring in tension ($\delta_{f,t}$) is selected as the horizontal distance from the bolt centerline to the edge of the plate or beam web, noting that no resistance can be provided once the bolt has passed beyond the edge of the plate or beam web. Computational simulations of bolt tear-out failure (Main and Sadek 2012, Section 3.1.3) have confirmed that this is a good estimate of the displacement at which the tear-out resistance reaches zero. No softening or element deletion is considered for bearing failure in compression. For axial behavior characterized by sudden fracture [Fig. 6(b)], a steeper drop in resistance after the ultimate load is considered, and the failure displacements of the spring in tension and

compression ($\delta_{f,t}$ and $\delta_{f,c}$, respectively) are set equal to $1.15\delta_u$, where the coefficient 1.15 was selected to avoid transient “ringing” that results from using a steeper drop in resistance in the explicit dynamic analysis. In the case of load reversal (e.g., if initial compressive forces in a connection spring due to flexural action later change to tensile forces due to catenary action), unloading follows a quadratic curve with no permanent offset (see Fig. 6) to represent the hysteresis associated with bolt shearing and bolt hole elongation. The unloading behavior does not have a significant effect for the prototype beam spans of 5.97 m or more considered subsequently. However, in comparisons with the experimental data described in the following section, with a beam chord length of only 1.97 m, compressive yielding occurred in the initial flexural response, and quadratic unloading was found to give better agreement with the data than linear unloading with the initial stiffness k .

The vertical shear behavior of each connection spring is represented using a load-deformation relationship of the form in Fig. 6(b), with symmetric behavior for upward and downward displacement. The yield and ultimate capacities of each spring (v_y and v_u , respectively) are obtained by dividing the vertical yield and ultimate capacities of the connection, calculated using equations in the AISC Specification (AISC 2010) with $\phi = 1$, by the number of bolts. The initial stiffness k and the displacement at the ultimate load, δ_u , are assumed to be the same in the vertical and axial directions, given by Eqs. (2) and (4), respectively, an approximation that was found to be reasonable based on numerical simulations (see Main and Sadek 2012). The failure displacement in vertical shear ($\delta_{f,v}$) is set to $1.15\delta_u$ regardless of the governing failure mode, conservatively assuming a rapid drop after the ultimate load in vertical shear. Interaction of the axial and shear failure modes is handled by deleting the connection spring from the model if the following inequality is satisfied:

$$\left(\frac{\delta_i}{\delta_{f,t}}\right)^2 + \left(\frac{\delta_{v,i}}{\delta_{f,v}}\right)^2 \geq 1 \quad (5)$$

where δ_i denotes the axial deformation and $\delta_{v,i}$ denotes the shear deformation of the i th connection spring element. Compressive failure is considered using a corresponding inequality, in which $\delta_{f,t}$ is replaced by

$\delta_{f,c}$. Note that while the ultimate capacities in axial tension, axial compression, and vertical shear may differ depending upon the governing failure modes, these criteria allow for failure of each biaxial connection spring due to any of the applicable failure modes. Failure of the connection occurs by successive failure of each spring element.

Comparison with Experimental Measurements

Thompson (2009) tested two-span beam assemblies with single-plate shear connections in the basic configuration illustrated in Fig. 1, but with pin connections at the exterior ends of the beams. A fairly short beam with a chord length of $L = 1.89$ m was used in these tests, where the chord length L denotes the horizontal distance between bolt centerlines. Half of the symmetrical test configuration is illustrated in Fig. 7, which shows a detailed model of an assembly with five bolts per connection. Three different connection sizes were considered, having three bolts, four bolts, and five bolts per connection. The bolt diameter, plate thickness, and other properties shown in Fig. 7 were the same for all connection sizes, except that the plate depth was 229 mm, 305 mm, and 381 mm for the 3-bolt, 4-bolt, and 5-bolt connections, respectively. In all cases the center of the top bolt was located 76.2 mm below the top of the beam. Three tests for each connection size were conducted for a total of nine tests. The same beams were used in all tests, with doubler plates welded to the beam webs in the connection regions to prevent bearing-induced deformations around the bolt holes in the beam web.

As illustrated in Fig. 7, the detailed models included only half of each assembly, with appropriate boundary conditions on the plane of symmetry through the center column. Modeling of the connection regions, including the center column, plate, beam, doubler plates, and bolts, followed the detailed modeling approach described previously, using solid elements and contact with friction. The test specimens used standard hole sizes for all bolts, for which the hole diameter is 1.6 mm larger than the bolt diameter. This gap was represented accurately in the solid element mesh, with the bolts initially centered in the holes and zero initial tension, allowing some slippage before bolt bearing is engaged. The beam span between connections, where stresses remain in the elastic range, was modeled using shell elements,

with nodal constraints linking the degrees of freedom of the solid and shell elements at their interface, indicated in Fig. 7. Because tensile test data were not available for the steel components used in these tests, representative stress-strain curves and failure strain values were used for the various types of steel, calibrated as described previously (Figs. 5 and 6).

Reduced models of the assemblies were also developed, following the approach outlined previously. As with the detailed model, only half of each assembly was modeled, with appropriate boundary conditions on the plane of symmetry. Axial load-deformation relationships used for the connection springs in the reduced model are shown in Fig. 8. The ultimate capacity was found to be governed by bolt shear failure in both tension and compression, and consequently, a sudden drop in resistance after the ultimate load is assumed, as in Fig. 6(b). The curves in Fig. 8 have zero load until a deformation of 1.6 mm in both tension and compression, in order to represent the initial gaps between the bolt shanks and the bolt holes, which allow some slippage to occur before bolt bearing is engaged. Including this initial gap is consistent with the detailed model and yields better agreement with the experimental data than if the gap is neglected. Initial gaps were included only in the axial load-deformation relationship, not in the vertical shear load-deformation relationship. Following the initial flat portion, the load increases with stiffness k from Eq. (2) and, after yielding, reaches the ultimate load at a deformation of δ_u from Eq. (4). The load-deformation relationships differ depending on the number of bolts in the connection, since both k and δ_u depend on d_b , the depth of the bolt group. A “gap element” was also introduced at the exterior pin support, allowing slippage of 1.6 mm before forces are developed. While bolt slippage has a relatively small effect for the prototype spans considered subsequently, its effect is more significant for the very short span length used in the experiments, because of the substantial compressive displacements imposed on the upper bolt rows in the initial flexural response. The inclusion of initial gaps thus influences the extent of compressive yielding and the subsequent unloading, which directly affects the development of axial forces in the beams.

Fig. 9 shows comparisons of experimental measurements with detailed and reduced model computations of (a) the vertical load P and (b) the beam axial force T versus the vertical displacement of the center column for the two-span beam assemblies with 4-bolt connections. Tests numbered 1, 2, and 3 in Fig. 9 correspond to tests 4ST1, 4ST2, and 4ST3 in Thompson (2009). The measured axial force T is an average of the axial forces measured in the two beam spans. Fig. 9 shows fairly good correspondence between the computational results and the experimental measurements, given the variability in the experimental data. Both the detailed and reduced models were able to capture the following primary stages in the response of the assemblies: (1) connection slippage, in which both the vertical load and the beam axial forces remain small before bolt bearing is engaged, (2) flexural action, in which the vertical load increases due to the development of bending moments in the single-plate shear connections, while the axial forces remain small, and (3) catenary action, in which tensile forces develop in the beams, accompanied by further increases in the vertical load until failure occurs. The results in Fig. 9 indicate that flexural action contributes significantly even at the initial drop in resistance associated with failure of the lowest bolt row. This is particularly evident in the detailed model results, where the peak vertical load occurs prior to the initial drop in resistance, even though larger values of axial tension are developed subsequently.

The detailed model computations showed that plastic deformations were concentrated in the bolts and in bearing-induced deformations around the bolt holes, as evidenced by the substantial shear deformation of about 4 mm shown in Fig. 10(b) for the bottom bolt and the significant elongation of bolt holes in the plates shown in Fig. 10(c). Outside of the connection region, the beam remained in the elastic range, essentially rotating as a rigid body, as evidenced by the straight-line deflected shape of the 4-bolt assembly at the ultimate load, shown in Fig. 10(a). While the failure mode predicted by the detailed and reduced models was bolt shear fracture in all cases, the failure mode varied from test to test in the experiments, even for nominally identical specimens, being bolt shear failure in some cases, tensile rupture of the plate in other cases, and block shear failure of the plate in still other cases. Calculations

based on Table 1 indicated an ultimate bearing capacity of the plate in tension only 8 % larger than the ultimate bolt shear capacity. The closeness of the calculated ultimate capacities helps to explain this observed variability in the failure mode, since typical variations in material strength could shift the failure from one component to another. While extensive bearing-induced elongations of the bolt holes were observed in all tests, the eventual failure modes were characterized by a steep drop in resistance after the ultimate load, which was captured by the detailed and reduced models (Fig. 9). The detailed and reduced models also captured the occurrence of successive failures, in which the resistance increased after an initial failure until a secondary failure occurred. In most tests, the peak vertical load P_u corresponded to the initial failure, as captured by the models, while test 1 of the 4-bolt assembly (Fig. 9) is a case in which the peak load corresponded to a secondary failure.

Quantitative comparisons of the computed and measured values of the ultimate vertical load P_u are presented in Table 2, which includes comparisons for the 4-bolt assembly based on results in Fig. 12, in addition to comparisons for the 3-bolt and 5-bolt assemblies based on similar results presented in Main and Sadek (2012). Table 2 shows that the detailed model results are within 15 % of the mean measured values, and the reduced model predictions are within 21 %, while the coefficient of variation in the measured values is as large as 20 %. This indicates that the deviations of the model predictions from the experimental measurements are comparable to the variability in the experimental measurements. The detailed models consistently underestimate P_u , while the reduced model overestimates P_u in one case by 10.6 %. Table 3 shows similar comparisons of the rotation at the ultimate load, θ_u , in which somewhat larger discrepancies are observed, with the computed rotations always being less than the experimental values. Note that the measured rotation values in Table 3, as well as those along the upper axes in Fig. 9, are about 5 % larger than the values reported by Thompson (2009). This is because the rotations in this study were calculated using the chord length of $L = 1.89$ m between bolt centerlines, for consistency with analytical models developed in Main and Sadek (2012), while Thompson (2009) used a length of 1.99 m from the exterior pin support to the face of the center column.

A number of factors likely contributed to the observed discrepancies between the experimental and computational results presented in Fig. 9 and in Tables 2 and 3. Flexibility of the reaction frame, which was not included in the models, may have contributed to the consistently larger rotations observed in the experiments as compared to the models (see Table 3). It is noted that Daneshvar and Driver (2011) achieved improved agreement between their detailed model predictions and the experimental measurements of Thompson (2009) by introducing axial springs at the exterior pin connections to represent the unknown flexibility of the reaction frame. The use of minimum specified strength values in the models (because measured material properties were unavailable), is another contributing factor, which would generally cause the models to underestimate the resistance of the connections. Differences between the detailed and reduced models result from the combined effect of the various approximations incorporated in the reduced models, including the use of Eq. (4), based on a fit to cyclic test data with inherent scatter, to estimate the deformation capacity of each bolt row.

Analysis of Shear Connections in Prototype Buildings

Table 4 summarizes the characteristics of gravity frames from two prototype steel frame buildings described in Main and Sadek (2012), which were developed to examine the influence of span length on disproportionate collapse resistance. The detailed design of the prototype buildings was carried out by a consulting engineering firm (Liang et al. 2006), with guidance and review by a panel of experts. Lateral loads are resisted by exterior moment frames, while all interior frames were designed to support gravity loads only. Beams and girders in the gravity frames were designed assuming fully composite action with the concrete slab, while it is noted that partially composite design is common in practice. ASTM A992 structural steel is used in the beams and columns, and beams in the gravity frames are connected to the columns using single-plate shear connections, illustrated in Fig. 11. In all connections, the center of the top bolt is placed 76.2 mm below the top of the beam, which is consistent with previous tests of single-plate shear connections (e.g., Liu and Astaneh-Asl 2004, Thompson 2009).

Influence of End Supports

Figs. 12 and 13 show comparisons of detailed and reduced model results computed for a two-span beam assembly with chord lengths of $L = 5.97$ m, corresponding to a N-S beam from building A. The results in Fig. 12 were computed with pin supports at the exterior ends of the beams, as in the tests by Thompson (2009), while the results in Fig. 13 were computed with two shear connections per span, as in the prototype structure. In all models, symmetry was exploited by analyzing only a single beam span. In the detailed models, shown in the insets of Figs. 12 and 13, the connection regions are represented using finely meshed solid elements, while the remainder of the beam span, where deformations are expected to be small, is represented using fairly coarse shell elements. Constraints are used to tie the edges of the shell elements to nodes of the solid elements at their interface. The A325 bolts are modeled using the stress-strain curve illustrated in Fig. 3, while the A36 steel plate and the A992 steel beam are modeled using the stress-strain curves in Fig. 4. For the detailed model with exterior pin supports (Fig. 12), an elastic material model is used for the shell elements surrounding the pin support, to preclude plastic deformations at that location. In the reduced models, calculations of yield and ultimate capacities based on Table 1 indicate axial behavior controlled by bearing and tear-out failure of the beam web, and a load-deformation relationship characterized by gradual softening [Fig. 6(a)] is used for the nonlinear connection springs.

Figs. 12 and 13 show good correspondence between the detailed and reduced model predictions, with differences of 4 % or less between the predictions of the peak vertical load and peak axial force. Both Figs. 12 and 13 show that the vertical load and axial force from the detailed model do not begin to increase significantly until the vertical column displacement exceeds about 80 mm. This occurs because the diameter of the bolt holes was modeled as 1.6 mm larger than the bolt diameter, while no pre-tension was applied to the bolts to introduce frictional clamping, so that some sliding occurs before the bolts come into bearing. This initial slippage was not included in the reduced models, in contrast with Fig. 8, so the reduced models show steeper increases in the vertical load and axial force initially. In spite of these initial discrepancies, the peak values of the vertical load and axial force agree quite closely.

Comparing Fig. 12 and Fig. 13 shows that the ultimate vertical load is about 30 % larger for the case with two shear connections per span (Fig. 13), while the peak axial force is about the same in both cases. The rotation at the ultimate vertical load is also about 30 % larger in Fig. 13, due to the additional axial deformation capacity provided by the exterior shear connections. Noting that the vertical component of the beam axial forces is given by $2T \sin \theta$, it follows that the same axial force occurring at a larger rotation results in a larger vertical load. It is thus observed that the greater axial deformation capacity provided by two shear connections per span results in substantial increases in both the ultimate load and the corresponding rotational capacity.

Influence of Span Length

Both the N-S and the E-W shear connections in building A have three A325 bolts and are nominally equivalent (see Table 4), except that the N-S beam has a slightly thicker web than the E-W beam, resulting in a bearing capacity in tension that is about 9 % greater. However, the span of the N-S beams is 6.1 m, while the span of the E-W beams is 9.1 m. Comparing the response of two-span beam assemblies from the N-S and E-W gravity frames of building A thus enables an assessment of the influence of span length on the behavior of the single-plate shear connections. Reduced models are used in this comparison, with load-deformation relationships characterized by gradual softening [Fig. 6(a)].

Fig. 14 shows a comparison of (a) the vertical load and (b) the beam axial force plotted against the rotation of the beam chord, θ , for the two assemblies with different span lengths. (Dual horizontal axes above the plots show the vertical displacement of the center column for the two different span lengths). While the peak axial force for the shorter span is only 7 % greater than for the longer span (a consequence of the slightly larger bearing capacity of the beam web), the difference in the vertical load capacity is significant, with the peak vertical load for the shorter span being 28 % greater than that for the longer span.

The displacement at ultimate load for the shorter span is about 20 % less than for the longer span. However, when beam chord rotations are considered, as indicated below the plots in Fig. 14, the rotation at ultimate load for the shorter span is actually about 18 % *greater* than that for the longer span. The rotational capacity is greater for the shorter span because the axial force for a given rotation is smaller, as shown in Fig. 14(b). Because the connections eventually fail primarily due to axial extension, the smaller axial forces for the shorter span enable the connection to sustain larger rotations prior to failure. Since the vertical component of the beam axial forces is given by $2T \sin\theta$, it follows that the same axial force occurring at a larger rotation results in a larger vertical load. It is thus observed that the greater rotational capacity of the shorter beam spans results in a substantial increase in the ultimate vertical load.

Influence of Connection Strength

The E-W gravity frames in buildings A and B have the same bay spacing of 9.1 m, but the E-W shear connections in building A have three bolts each, while those in building B have four bolts each.

Comparing the response of two-span beam assemblies from the E-W gravity frames of buildings A and B thus enables an assessment of the influence of the number of bolts, or the connection strength, on the behavior of the single-plate shear connections. Reduced models are used in this comparison, with load-deformation relationships characterized by gradual softening [Fig. 6(a)].

Fig. 15 shows a comparison of (a) the vertical load and (b) the beam axial force plotted against the vertical displacement of the center column for the two assemblies with different numbers of bolts per connection. The peak vertical load for the four-bolt connection is twice as large as that of the three-bolt connection, while the peak axial force is 1.8 times larger. It is thus observed that the vertical capacity of the assembly with four-bolt connections is substantially larger than that of the assembly with three-bolt connections, due primarily to the increased axial capacity of the connections. Note that the axial capacity of the four-bolt connection is more than $1\frac{1}{3}$ times that of the three-bolt connection because, in addition to the larger number of bolts, the four-bolt connection has a thicker beam web (the beam web thickness, denoted t_w , is indicated in Fig. 15). This changes the failure mode from tear-out through the beam web to

tear-out through the plate, resulting in bearing capacities for each bolt that are 45 % larger. The displacement (or rotation) at ultimate load is comparable in the two cases, being about 6 % larger for the four-bolt connection than for the three-bolt connection. Note that for rotation without axial extension, the rotation at the ultimate load would be smaller for the four-bolt connection, according to Eq. (3). The influence of axial extension on rotational capacities under column loss is further discussed subsequently.

Influence of Post-Ultimate Behavior

To investigate the influence of post-ultimate behavior, two-span beam assemblies from the prototype buildings, which were analyzed previously assuming a gradual softening behavior [Fig. 6(a)], were analyzed again assuming that sudden fracture occurs when the ultimate load of each bolt row is reached [Fig. 6(b)]. The parameters of the reduced connection models in these analyses were the same as those used previously, except that the failure displacement in tension was reduced to $1.15\delta_i$ in all cases.

Fig. 16 shows a comparison of (a) the vertical load and (b) the beam axial force plotted against the vertical displacement of the center column for two-span beam assemblies with the alternate post-ultimate behaviors. These results correspond to the E-W gravity frames of building B, with a bay spacing of 9.1 m and with four A325 bolts per connection. Similar results were obtained for the N-S and E-W gravity frames of building A (see Main and Sadek 2012). In all cases the peak vertical load is significantly less for sudden fracture than for gradual softening, being 16 % less for the E-W gravity frames of building B [Fig. 16(a)] and 23 % less for the N-S gravity frames of building A (not shown). The peak axial forces are only slightly less for sudden fracture than for gradual softening, being only 2 % less in Fig. 16(b). However, the axial forces are sustained for larger rotations in the case of gradual softening, resulting in larger vertical loads since the vertical component of the beam axial forces is given by $2T \sin\theta$. It is thus observed that the connections characterized by gradual softening achieve increased vertical load capacity by sustaining comparable levels of axial tension under larger rotations.

Rotational Capacities

Fig. 17 shows beam chord rotations at initial failure from the experiments of Thompson (2009) plotted against the depth of the bolt group, d_{bg} , along with the corresponding rotations at initial failure from the detailed and reduced models of these tests (see Fig. 9). Initial failure in the reduced models corresponds to the rotation at which the bottom bolt reaches its ultimate load, corresponding to a deformation of δ_u . Also plotted in Fig. 17 is the expression for θ_{max} from Eq. (3), which is based on linear regression of data from cyclic flexural testing of simple shear connections reported in FEMA 355D (FEMA 2000). Recall that δ_u , defined in Eq. (4), was obtained directly from θ_{max} by assuming pure rotation of the connection about the center of the bolt group in the cyclic testing. Fig. 17 shows that the rotations at initial failure are significantly less than θ_{max} , being 35 % less for the reduced model of the 5-bolt connection. This indicates that the combination of rotation and axial extension due to column loss causes the bottom bolt row to reach its ultimate load at a smaller rotation than under pure rotation.

Fig. 18 shows beam chord rotations at the peak vertical load, from the reduced model results in Fig. 15, plotted against the depth of the bolt group, d_{bg} , along with the linear regression equation for θ_{max} from Eq. (3). Reduced model results are shown for both gradual softening and sudden fracture (see Fig. 16), with the rotational capacities being about 16 % less in the latter case. Note that the rotational capacities in Fig. 18 are lower than those shown in Fig. 17, because the longer beam span of Fig. 18 imposes greater deformations on the connections for a given chord rotation θ . Due to differences in the kinematics of the assembly with two shear connections per span as compared to the assembly with exterior pin supports at beam mid-height (i.e., the exterior pin support prevents axial displacement and constrains rotations about the beam mid-height rather than about the center of the bolt group; see Main and Sadek 2012), the reduced model results in Fig. 18 (with two shear connections per span) show a slight increasing trend of rotational capacity with d_{bg} , in contrast with the decreasing trend shown in Fig. 17 (with exterior pin supports at beam mid-height). The rotational capacities from the reduced models in Fig. 18 are significantly less than predicted by FEMA 355D (FEMA 2000), being as much as 62 % less

than θ_{\max} for the 3-bolt connection with sudden fracture. In the case of pure rotation, the reduced models would yield exactly the same rotational capacities as θ_{\max} from FEMA 355D, since the deformation capacity of each bolt row in Eq. (4) was evaluated directly from θ_{\max} in Eq. (3). The results in Fig. 18 thus clearly show that the axial extensions imposed under column loss scenarios lead to significant reductions in the rotational capacities of the connections.

Conclusions

Two alternative modeling approaches were described for analysis of single-plate shear connections under column loss: (1) detailed modeling and (2) reduced modeling. The detailed modeling approach used solid elements, contact algorithms, and plasticity models calibrated to match stress-strain curves and fracture strains from tensile tests. The reduced modeling approach used an assembly of nonlinear spring elements, extending the model of Sadek et al. (2008) by incorporating shear failure, connection slippage, inelastic unloading behavior, and the possibility of sudden fracture. Both detailed and reduced models were compared with experimental data from push-down tests of two-span beam assemblies by Thompson (2009), and fairly good agreement was observed, with deviations in the ultimate vertical load being comparable to the variability in the measurements themselves. The models were able to capture successive stages of the measured responses, including (1) connection slippage, (2) flexural action, and (3) catenary action, in which tensile forces developed in the beams and increased until failure occurred.

The models were then used to investigate the influence of various factors on the behavior of two-span beam assemblies from prototype gravity framing systems. Comparing assemblies with (1) exterior pin supports, as in the tests by Thompson (2009), and (2) two shear connections per span, as in a typical gravity framing system, showed that the additional axial deformation capacity provided by exterior shear connections produced increases of 30 % in both the ultimate vertical load and the corresponding rotational capacity. Comparing assemblies with spans of 6.1 m and 9.1 m, with comparable 3-bolt connections, showed the ultimate vertical load to be 28 % greater for the shorter span, due to the smaller deformations imposed on the connections for a given rotation. Comparing assemblies with 3-bolt and 4-

bolt connections, both with 9.1 m spans, showed the ultimate vertical load to be about twice as large with the 4-bolt connections, due to primarily to the increased tensile capacity of the connections. The increased tensile capacity of the 4-bolt connections was due not only to the additional bolt, but also to an increased tear-out capacity per bolt because of the thicker beam web. Comparing assemblies with post-ultimate behavior characterized by gradual softening (typical of bolt tear out) and sudden fracture (typical of bolt shear rupture) showed the ultimate vertical load to be as much as 23 % less in the case of sudden fracture. Based on this significant reduction and the prevalence of sudden fractures observed experimentally (Thompson 2009, Weigand et al. 2012), it is recommended that sudden fracture, rather than gradual softening, should be assumed in the analysis of single-plate shear connections. Rotational capacities of single-plate shear connections under column loss were found to be as much as 62 % less than those based on seismic testing of shear connections (FEMA 2000), due to the axial component of extension imposed in addition to rotation.

Acknowledgments

Christopher H. Raebel and Scott L. Thompson of the Milwaukee School of Engineering are gratefully acknowledged for providing experimental data from their tests of two-span beam assemblies with single-plate shear connections. Valuable comments and input on this work were provided by H.S. Lew (NIST) and Judy Liu (Purdue University).

Disclaimers

Certain commercial entities, equipment, products, or materials are identified in this document in order to describe a procedure or concept adequately. Such identification is not intended to imply recommendation, endorsement, or implication that the entities, products, materials, or equipment are necessarily the best available for the purpose. The policy of the National Institute of Standards and Technology is to include statements of uncertainty with all NIST measurements. In this document, however, measurements of authors outside of NIST are presented, for which uncertainties were not reported and are unknown.

References

- Alashker, Y., El-Tawil, S. and Sadek, F. (2010). "Progressive Collapse Resistance of Steel-Concrete Composite Floors." *Journal of Structural Engineering*, 136(10), 1187-1196.
- American Institute of Steel Construction (AISC). (2010). "Specification for Structural Steel Buildings." *ANSI/AISC 360-10*, Chicago, IL.
- Daneshvar, H. and Driver, R.G. (2011). "Behavior of shear tab connections under column removal scenario." *Proc., 2011 Structures Congress*, American Society of Civil Engineers, Reston, VA.
- Federal Emergency Management Agency (FEMA). (2000). "State of the art report on connection performance." *FEMA 355D*, SAC Joint Venture and FEMA, Washington, D.C.
- Hallquist, J. (2007). "LS-DYNA Keyword User's Manual." Livermore Software Technology Corporation, Livermore, CA.
- Kulak, G. L., Fisher, J. W., and Struik, J. H. A., (1986). *Guide to Design Criteria for Bolts and Riveted Joints*, 2nd Ed., John Wiley & Sons, New York.
- Liang, X., Shen, Q., and Ghosh, S.K. (2006). "Assessing the ability of seismic structural systems to withstand progressive collapse: Design of steel frame buildings." *Report submitted to the Building and Fire Research Laboratory*, National Institute of Standards and Technology, Gaithersburg, MD.
- Liu, J. and Astaneh-Asl, A. (2004). "Moment-rotation parameters for composite shear tab connections." *Journal of Structural Engineering*, 130(9), 1371-1380.
- Main, J.A. and Sadek, F. (2012). "Robustness of steel gravity frame systems with single-plate shear connections." *NIST Technical Note 1749*, National Institute of Standards and Technology, Gaithersburg, MD. <<http://dx.doi.org/10.6028/NIST.TN.1749>> (accessed October 10, 2012)
- Oosterhof, S.A. and Driver, R.G. (2012). "Performance of steel shear connections under combined moment, shear, and tension." *Proc., 2012 Structures Congress*, American Society of Civil Engineers, Reston, VA.
- Research Council on Structural Connections (RCSC). (2004). *Specifications for Structural Joints Using ASTM A325 or A490 Bolts*, AISC, Chicago.

- Rex, C.O., and Easterling, S.W. (2003). "Behavior and modeling of a bolt bearing on a single plate." *Journal of Structural Engineering*, 129(6), 792-800.
- Richard, R.M., Gillett, P.E., Kriegh, J.D., and Lewis, B.A. (1980). "The analysis and design of single plate framing connections." *Engineering Journal*, AISC, 2nd Quarter, 38-52.
- Sadek, F., El-Tawil, S., and Lew, H.S. (2008). "Robustness of composite floor systems with shear connections: modeling, simulation, and evaluation." *Journal of Structural Engineering*, 134(11), 1717-1725.
- Sadek, F., Main, J. A., Lew, H. S., Robert, S. D., Chiarito, V. P., and El-Tawil, S. (2010). "An Experimental and Computational Study of Steel Moment Connections under a Column Removal Scenario." *NIST TN 1669*, National Institute of Standards and Technology, Gaithersburg, MD.
- Sarraj, M. (2007). "The behaviour of steel fin plate connections in fire." Ph.D. Dissertation, The University of Sheffield, Sheffield, UK.
- Thompson, S.L. (2009) "Axial, shear and moment interaction of single plate 'shear tab' connections." Master's Thesis, Milwaukee School of Engineering, Milwaukee, WI.
- Wallaert, J.J., and Fisher, J.W. (1965). "Shear strength of high-strength bolts." *Journal of the Structural Division, ASCE*, Vol. 91, ST3, 99-125.
- Weigand, J.M., Meissner, J.E., Francisco, T., Berman, J.W., Fahnestock, L.A., and Liu, J. (2012). "Overview of AISC/NSF structural integrity research and preliminary results." *Proc., 2012 Structures Congress*, American Society of Civil Engineers, Reston, VA.
- Yim, H.C. and Krauthammer, T. (2012). "Mechanical properties of single-plate shear connections under monotonic, cyclic, and blast loads." *Engineering Structures*, 37, 24-35.

Tables

Table 1. Equations used to calculate yield and ultimate capacities of single bolt rows in tension and compression

Failure Mode	Tensile Capacities		Compressive Capacities	
	t_y (yield)	t_u (ultimate)	c_y (yield)	c_u (ultimate)
Bearing at bolt hole	$1.5L_ctF_y \leq 3.0dtF_y$	$1.5L_ctF_u \leq 3.0dtF_u$	$3.0dtF_y$	$3.0dtF_u$
Bolt shear*	$0.75F_vA_b$	F_vA_b	$0.75F_vA_b$	F_vA_b

* $F_v = 517$ MPa (75 ksi) for ASTM A325 bolts and $F_v = 646$ MPa (94 ksi) for ASTM A490 bolts, both with threads excluded from the shear plane.

Table 2. Comparison of model predictions and experimental measurements (Thompson 2009) of ultimate vertical load P_u for two-span beam assemblies

Connection Size	Detailed Model		Reduced Model		Experiment	
	P_u	[Deviation*]	P_u	[Deviation*]	Mean P_u	[COV [†]]
3 bolts	47.1 kN	[-14.6 %]	43.4 kN	[-21.3 %]	55.1 kN	[11.3 %]
4 bolts	65.7 kN	[-10.6 %]	74.8 kN	[+1.8 %]	73.5 kN	[19.5 %]
5 bolts	90.7 kN	[-5.8 %]	106.6 kN	[+10.6 %]	96.4 kN	[7.1 %]

* Percentage deviation from mean experimental value

[†] Coefficient of Variation = [standard deviation]/[mean]

Table 3. Comparison of model predictions and experimental measurements (Thompson 2009) of rotation at ultimate load, θ_u , for two-span beam assemblies

Connection Size	Detailed Model		Reduced Model		Experiment	
	θ_u	[Deviation*]	θ_u	[Deviation*]	Mean θ_u	[COV [†]]
3 bolts	0.120 rad	[-13.8 %]	0.103 rad	[-26.1 %]	0.139 rad	[3.4 %]
4 bolts	0.087 rad	[-21.5 %]	0.093 rad	[-16.6 %]	0.111 rad	[18.8 %]
5 bolts	0.066 rad	[-24.3 %]	0.082 rad	[-5.6 %]	0.087 rad	[9.6 %]

* Percentage deviation from mean experimental value

† Coefficient of Variation = [standard deviation]/[mean]

Table 4. Beam spans, shapes, and number of bolts per connection in gravity frames of prototype buildings

Building	Direction	Span	Shape	Bolts
A	East-West	9.14 m	W14×22	3
	North-South	6.10 m	W16×26	3
B	East-West	9.14 m	W21×50	4
	North-South	10.16 m	W16×26	3

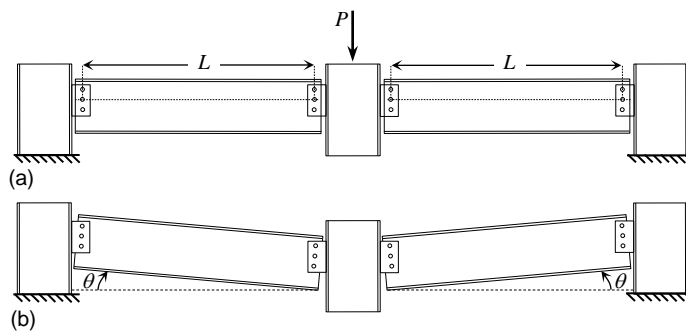


Fig. 1. Two-span beam assembly under pushdown loading with unsupported center column:
(a) original configuration; (b) deformed configuration.

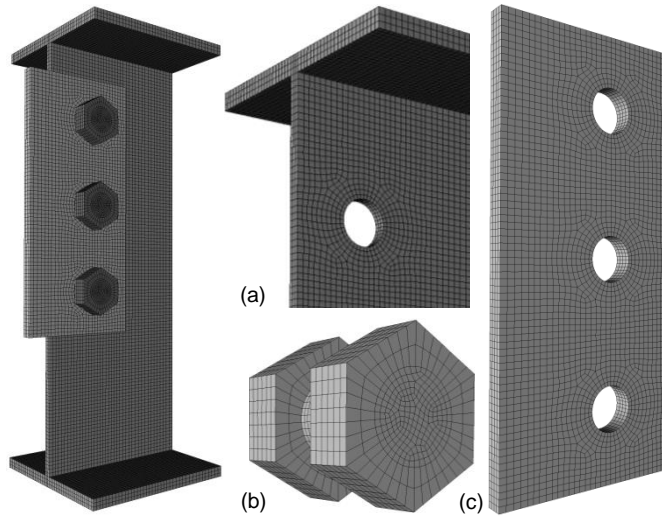


Fig. 2. Detailed model of single-plate shear connection showing finite element mesh of (a) beam, (b) bolt, and (c) shear tab

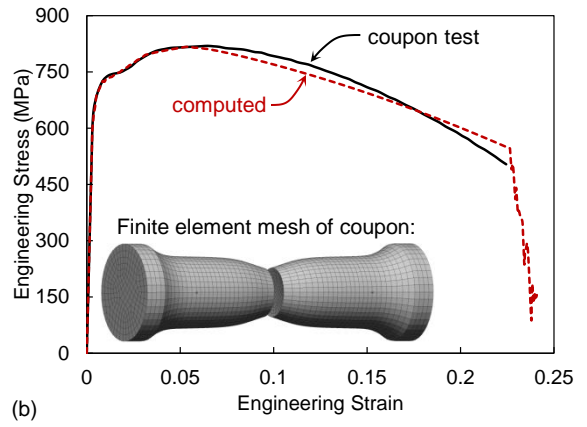
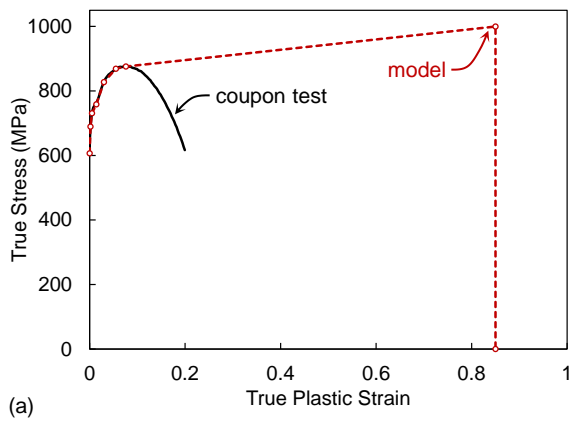


Fig. 3. (a) True stress-strain and (b) engineering stress-strain curves for A325 bolt material

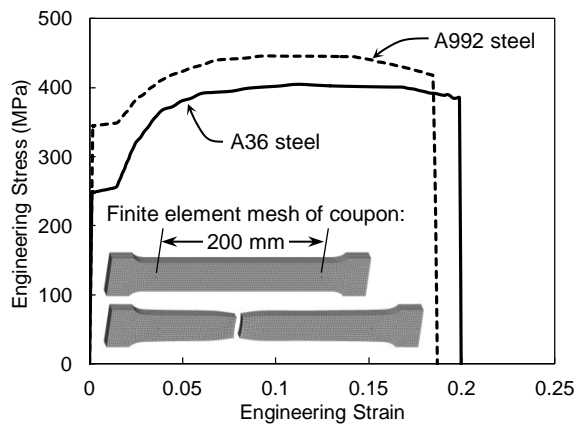


Fig. 4. Stress-strain curves used to represent A36 and A992 steel in detailed models

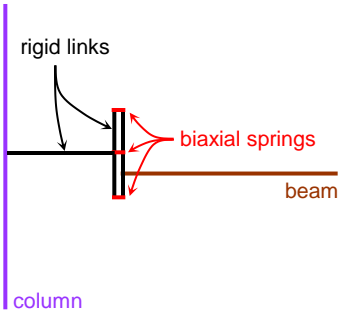


Fig. 5. Reduced model of single-plate shear connection.

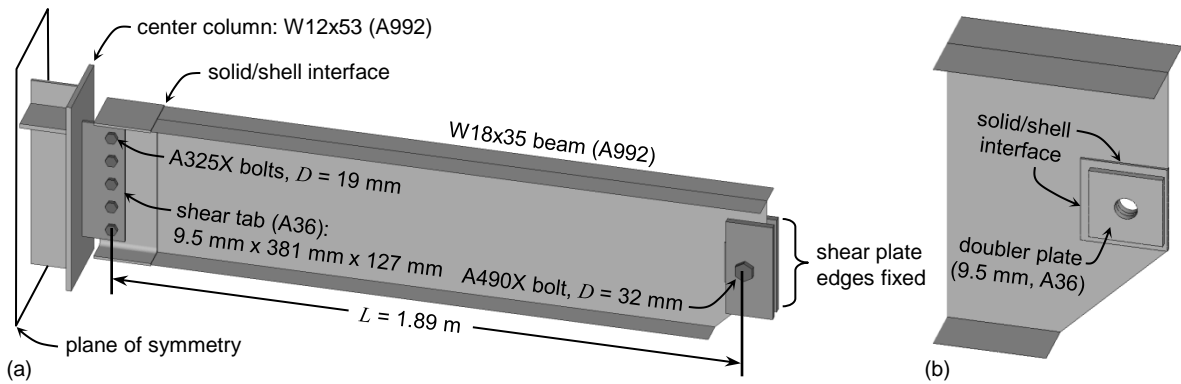


Fig. 7. Detailed model of two-span beam assembly tested by Thompson (2009):
 (a) overview; (b) region near exterior pin connection

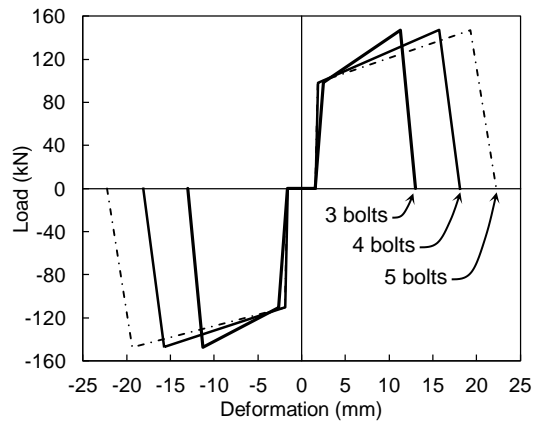


Fig. 8. Axial load-deformation relationships used in reduced models of connections tested by Thompson (2009)

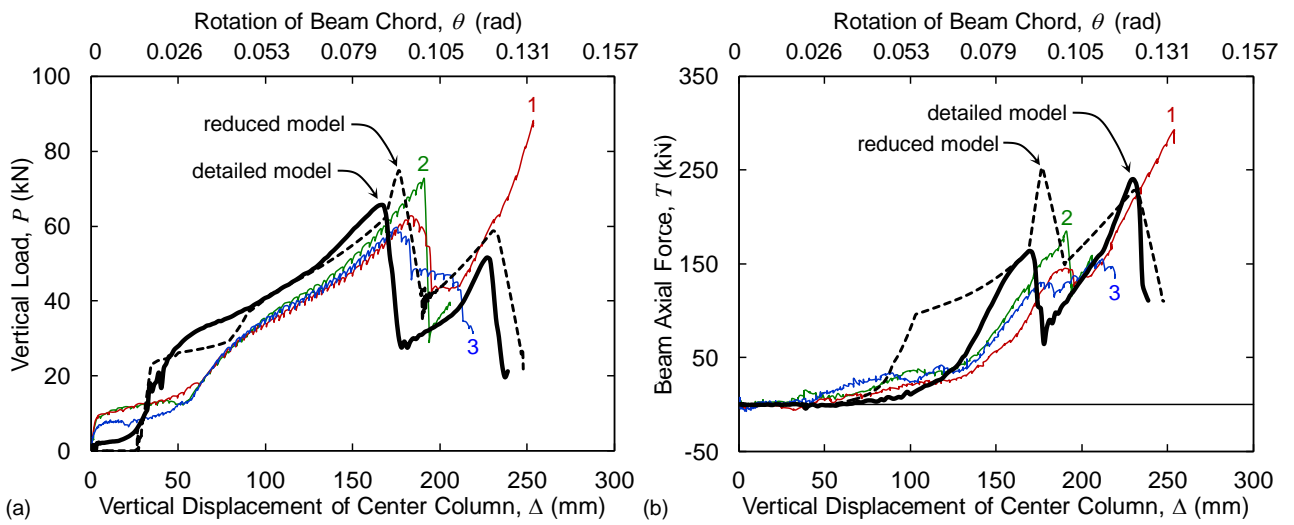


Fig. 9. Comparison of computed results with experimental data (Thompson 2009) for two-span beam assemblies with 4-bolt connections: (a) vertical load and (b) axial force versus vertical column displacement (numerical labels on curves indicate test number)

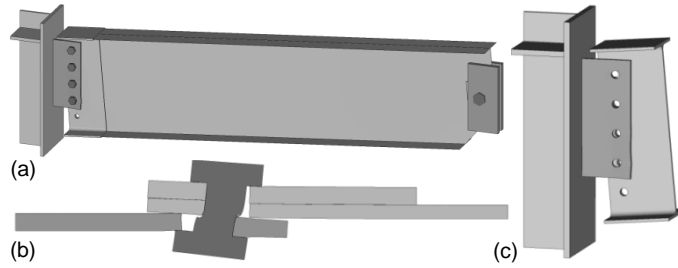


Fig. 10. Deformations of 4-bolt assembly at ultimate load: (a) overview; (b) section view through bottom bolt; (c) connection region (bolts hidden)

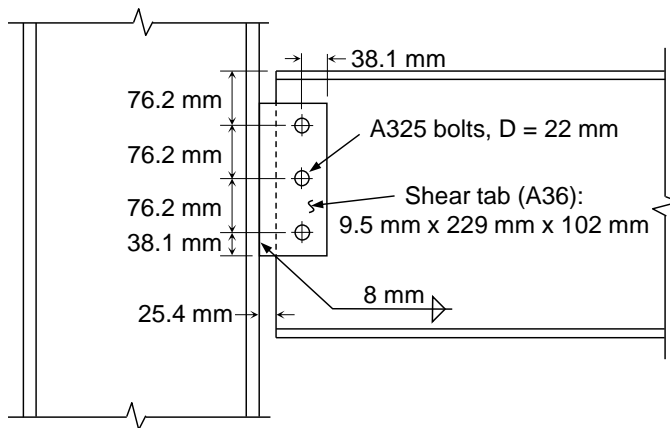


Fig. 11. Details of prototype single-plate shear connection

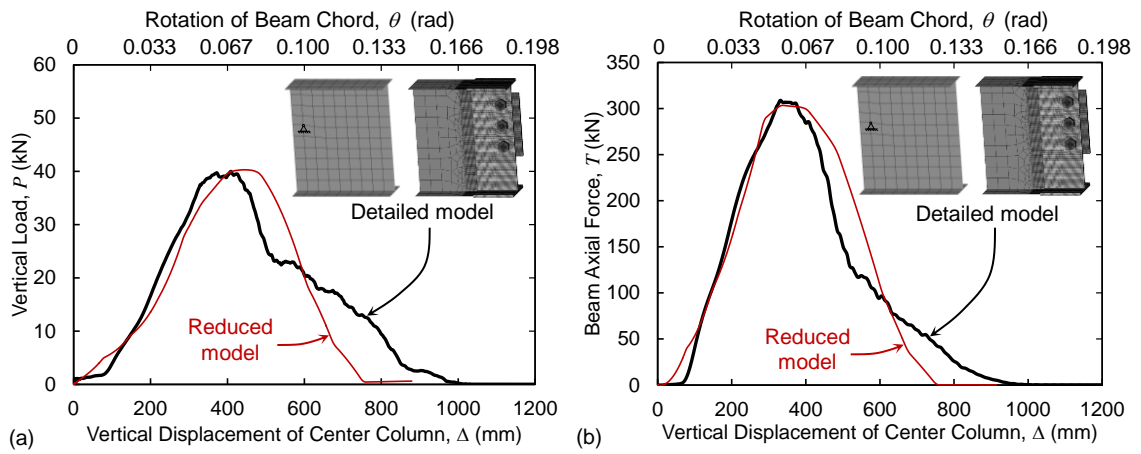


Fig. 12. Comparison of detailed and reduced model results for two-span beam assembly with exterior pin supports: (a) vertical load and (b) axial force versus vertical column displacement

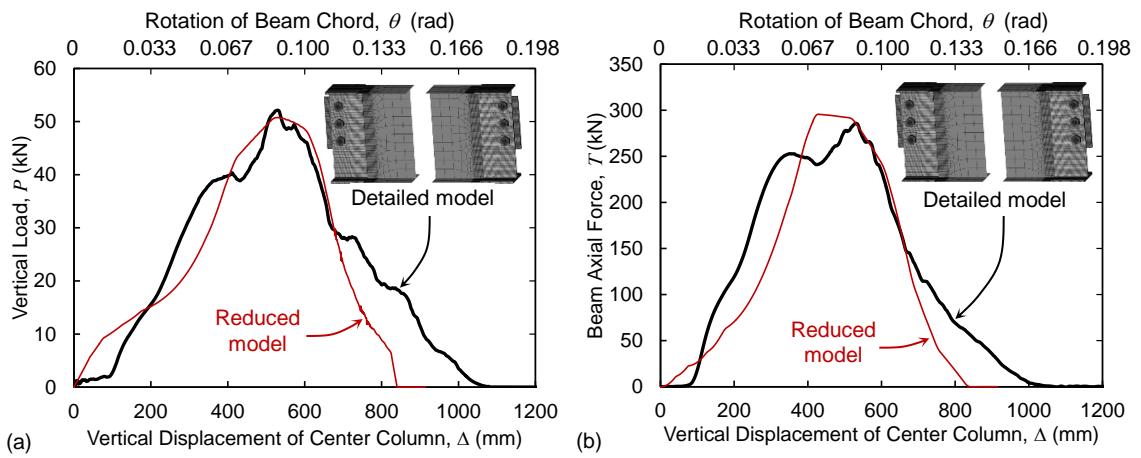


Fig. 13. Comparison of detailed and reduced model results for two-span beam assembly with two shear connections per span: (a) vertical load and (b) axial force versus vertical column displacement

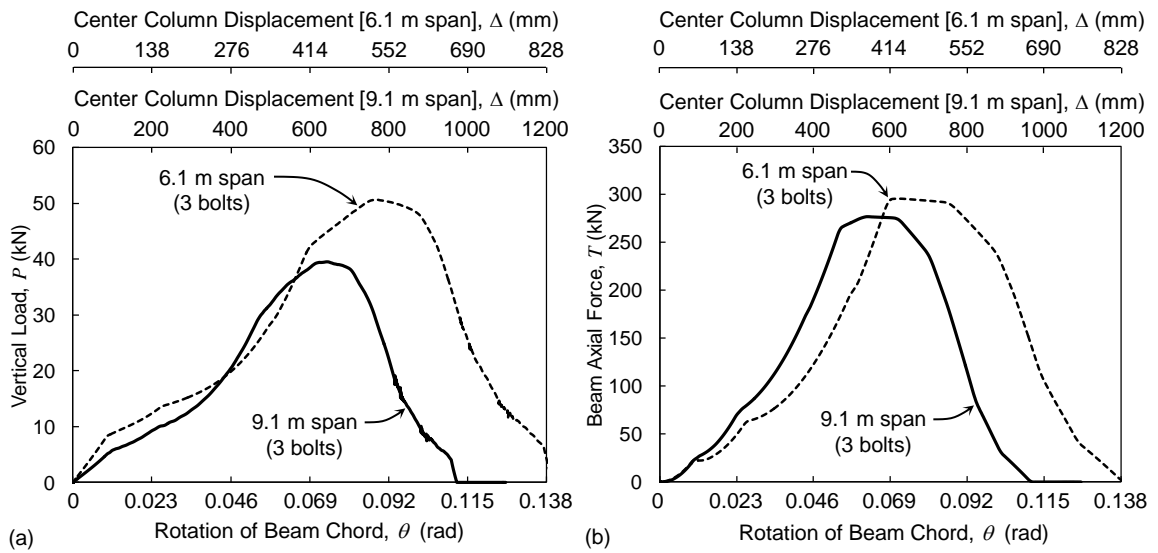


Fig. 14. (a) Vertical load and (b) beam axial force vs. beam chord rotation for different span lengths

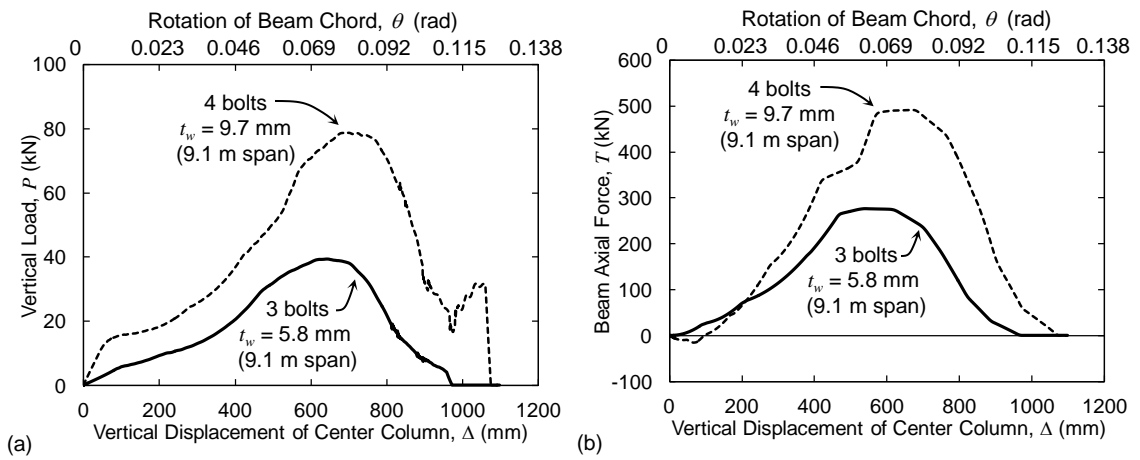


Fig. 15. (a) Vertical load and (b) beam axial force vs. center column displacement for 9.1 m beam spans with different connection strengths

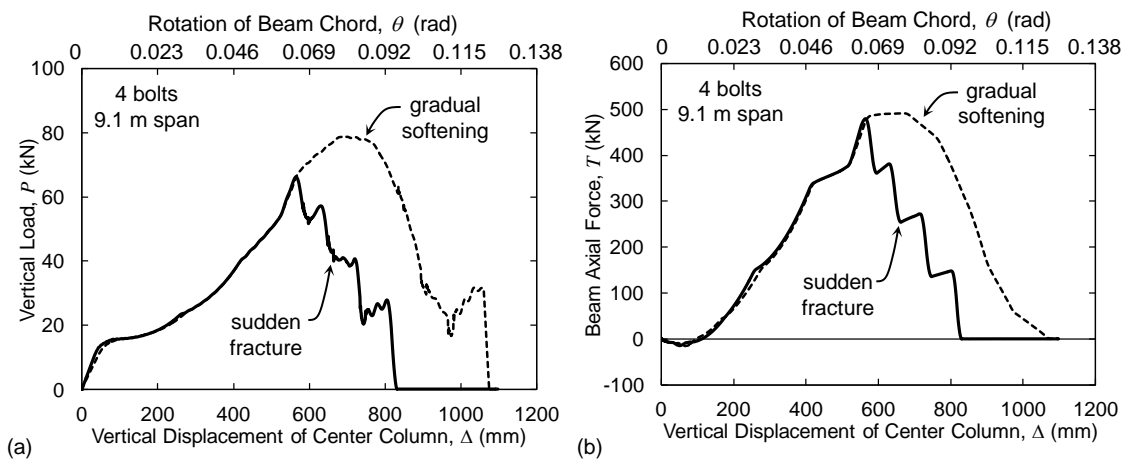


Fig. 16. (a) Vertical load and (b) beam axial force vs. center column displacement for connections with different post-ultimate behavior

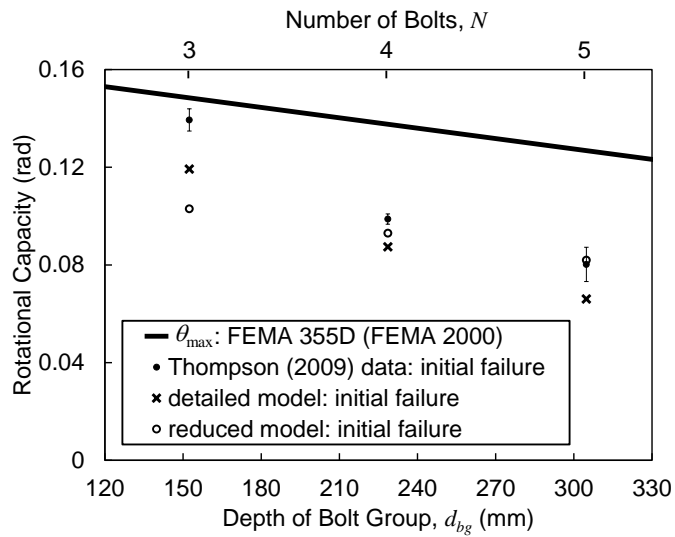


Fig. 17. Comparison of experimental and computed rotational capacity values with best-fit line based on seismic test data ($L = 1.89$ m, exterior pin supports; solid circles indicate mean experimental values and error bars indicate maximum and minimum values from a series of three tests)

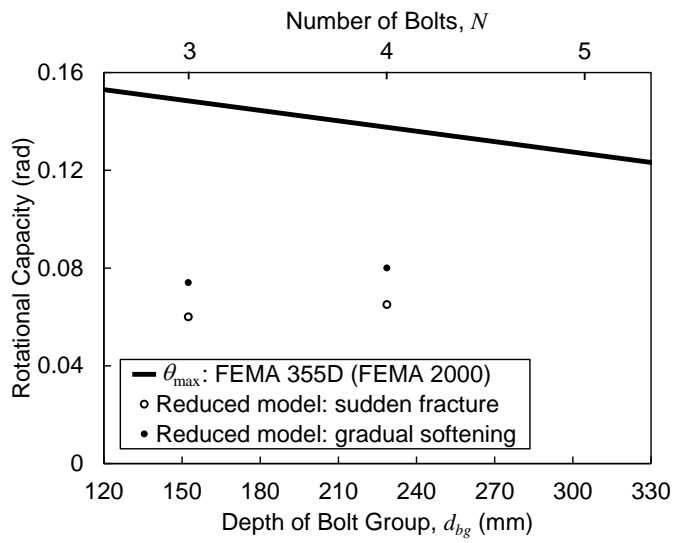


Fig. 18. Comparison of computed rotational capacities with best-fit line based on seismic test data (9.1 m span, two shear connections per span)